Behavior of Negative Ion and Secondary Particles in Multi-Aperture Accelerator*)

Masashi KISAKI, Pierluigi VELTRI[1)], Piero AGOSTINETTI[1)], Katsuyoshi TSUMORI, Katsunori IKEDA, Haruhisa NAKANO, Gianluigi SERIANNI[1)], Masaki OSAKABE, Kenichi NAGAOKA, Yasuhiko TAKEIRI and Osamu KANEKO

National Institute for Fusion Science, Toki 509-5292, Japan
[1)]*Consorzio RFX, Padova, 35126, Italy*

(Received 7 December 2012 / Accepted 6 March 2013)

The trajectories of the H^- and the secondary particle in a multi-aperture accelerator for negative ion sources were calculated with a 3D numerical code, taking into account non-uniformity in magnetic field and negative ion density, and the heat loading on acceleration grids was estimated. The heat loading on a grounded grid mainly originates from the secondary electron impact and the non-uniform transverse magnetic field enhances the possibility of the secondary electron impacts on the grounded grid. Perveance condition of beamlets strongly depends on the plasma density profile and the direct interception of the H^- by an extraction grid is enhanced in the non-uniform plasma case.

Keywords: negative ion source, NBI, accelerator, charged particle beam, numerical calculation

DOI: 10.1585/pfr.8.2405060

1. Introduction

The negative-ion-based neutral beam injection (N-NBI) system is expected to be the main heating device for magnetically confined plasma. A neutral hydrogen beam of more than 15 MW is successfully injected by three N-NBIs on Large Helical Device (LHD). One of the key issues for extending the beam power and pulse length is the reduction of heat loadings on acceleration grids and beamline components, which are mainly caused by secondary particles produced in the accelerator.

Negative ion sources for fusion experiments have large-sized and multi-aperture grids [1–3]. It is foreseen that the negative ions are distributed non-uniformly in the source [4] and magnetic field usually has the complicate configuration in the accelerator [5]. In previous studies, only the behavior of the stripped electron in non-uniform magnetic field has been investigated in detail [5], but the trajectory of the other secondary particles has been calculated in the single-aperture model [6, 7], which assumes that the negative ions are extracted with the same current density in each aperture and the magnetic field is uniformly created in whole area. Therefore, a large discrepancy between experiments and simulations is observed though the experimental and numerical studies have been carried out intensely.

The accelerator of the LHD-NBI is modeled with a 3D numerical code aiming for better understanding of the behavior of H^- and secondary particle in the multi-aperture accelerator. Trajectories of H^- and secondary particle through multi-apertures are calculated and the grid heat loading is estimated. In this paper, the influence of non-uniformity in the magnetic field and the source plasma on trajectories of the H^- and the secondary particles will be presented.

2. LHD-NBI

Figure 1 (a) shows a cross-sectional view of a N-NBI on LHD. The N-NBI consists of a plasma chamber and an electrostatic accelerator. The dimension of the chamber is 35 cm in width, 145 cm in height and 22 cm in depth. The hydrogen plasma is generated by the arc discharge with 24 tungsten filaments and confined by the cusp magnetic field. The transverse magnetic field is formed by filter magnets in order to divide the chamber into two regions, a driver region and an extraction region. Figures 1 (b) and (c) show schematic illustrations of the accelerator and the accelerator grid segments, respectively. The accelerator is composed of 4 grids: plasma grid (PG), extraction grid (EG), steering grid (SG), and grounded grid (GG). Each grid is divided into 5 segments, 25 cm in height and 30 cm in width, and 11 (vertical) $\times$ 14 (horizontal) apertures are drilled on a segment. Electron deflection magnets, whose magnetized direction changes alternately from row to row, are embedded in the EG and strong magnetic field is produced locally in order to prevent electrons extracted with H^- from being fully accelerated and dumping the high power load on beamline components. This field also de-

author's e-mail: kisaki.masashi@LHD.nifs.ac.jp
*) This article is based on the presentation at the 22nd International Toki Conference (ITC22).

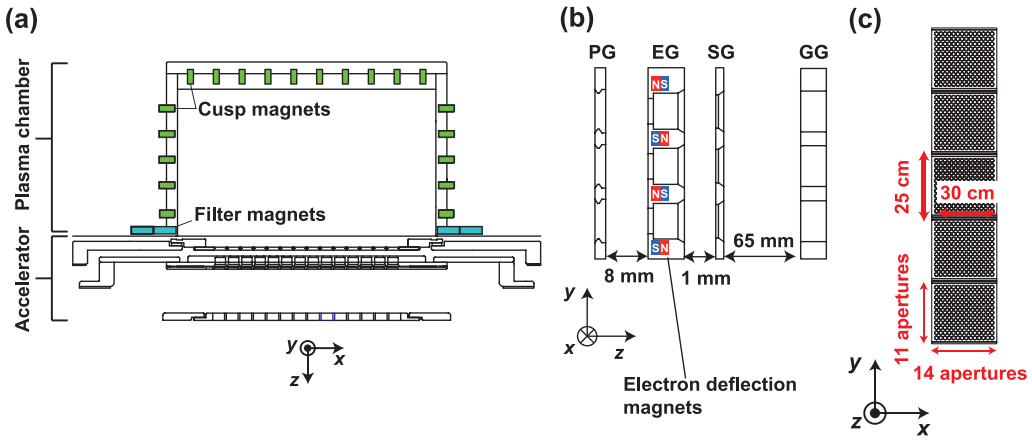

Fig. 1 Schematic illustrations of (a) N-NBI on LHD, (b) accelerator, and (c) acceleration grid.

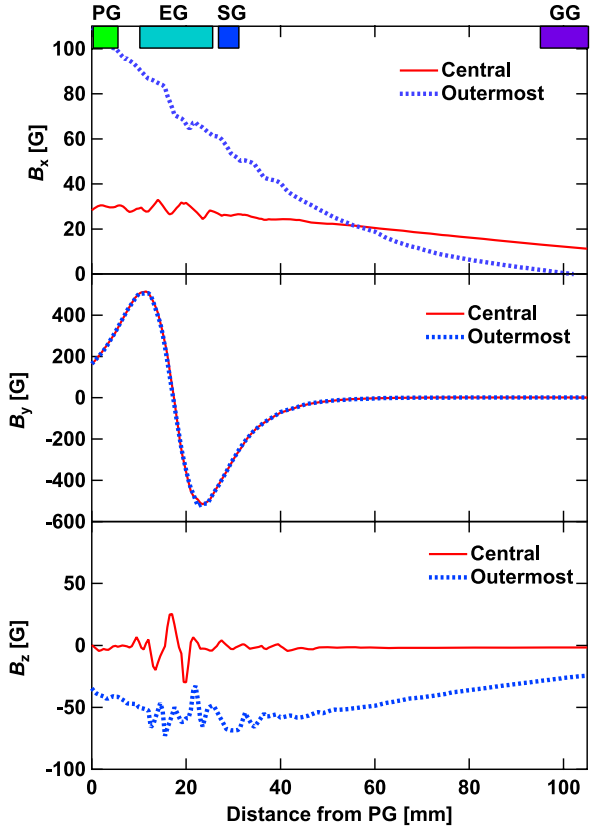

Fig. 2 Magnetic field as a function of distance from plasma grid in accelerator. Solid and dotted lines show magnetic field through central and outmost apertures, respectively.

flects the extracted beamlets slightly. In order to compensate the beam deflection and focus the multi-beamlets properly, apertures on the SG and the GG are displaced [8].

Figure 2 shows the calculated magnetic field in the accelerator as a function of the distance from the PG. The strong magnetic field of Y component is formed locally near the EG by the electron deflection magnets and has horizontally uniform profile. On the other hand, horizontally non-uniform magnetic fields of X and Z components are formed due to filter magnets. The B_x and the B_z in the

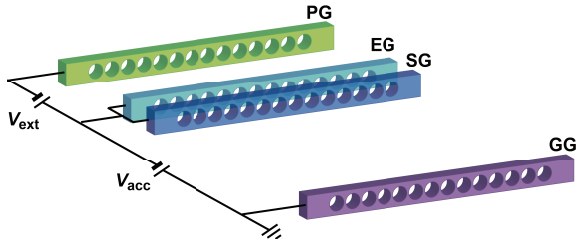

Fig. 3 Multi-aperture accelerator modeled for particle trajectory calculation.

outmost aperture in x direction are stronger than that in the central aperture.

3. Calculation Model

In the accelerator, several types of particles (i.e., electrons, positive ions, and neutrals) are created when the extracted H^- beam collides with residual background gas. Charged particles are accelerated and deflected by the electromagnetic field. Some fractions of secondary particles and H^- impinges on acceleration grids and yields secondary electrons. To simulate these processes in the accelerator, Electrostatic Accelerator Monte Carlo Code (EAMCC) [9] is applied to the N-NBI on LHD. EAMCC calculates interactions of test particles including H^- and secondary particle with the residual gas and acceleration grids using the Monte Carlo techniques.

EAMCC does not derive the electromagnetic field created by the related charged particles self-consistently, but reads the electric potential and magnetic field maps obtained with other simulation codes to track test particles. In this study, the electric potential map is calculated with OPERA-3d [10] and SLACCAD [11], which is used for calculating the potential in the first gap between the PG and the EG, and the magnetic field map is obtained with OPERA-3d. OPERA-3d is a 3 dimensional electromagnetic analysis code and simulates the beam trajectory in the electrostatic field taking into account space charge effect

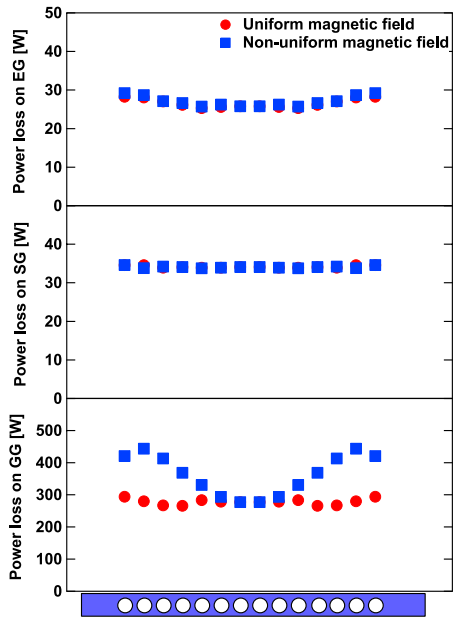

Fig. 4 Power loss of particles on acceleration grids in (●) uniform and (■) non-uniform magnetic field cases.

of the beam. Therefore, the beamlet-beamlet interaction can be calculated. Figure 3 shows a calculation model for OPERA-3d. To obtain the electric potential created by the multi-beamlets of H^- extracted from non-uniform plasma, a row of 14 horizontal apertures is modeled. Vext is the extraction voltage and Vacc is the acceleration voltage. Since OPERA-3d is the full 3D numerical code, the aperture displacements in the SG and GG are taken into account. In the OPERA simulation, the magnetic field produced by filter magnets and electron deflection magnets is also included.

4. Calculation Results

4.1 Influence of non-uniform magnetic field on secondary particle trajectory

Secondary particle trajectories in non-uniform magnetic field were calculated with the electric potential map obtained on the uniform plasma condition, where 14 beamlets with the current density of 30 mA/cm^2 are extracted at the extraction voltage of 9.6 kV and the acceleration voltage of 178 kV. Figure 4 shows the power loss of the H^- and secondary particle on acceleration grids in each aperture for uniform and non-uniform magnetic field cases. Note that in the uniform field case, the magnetic field map in the central aperture was used for other apertures. Stripping reactions mainly occur in the first gap because of higher residual gas density and the cross section for the reaction, which have a peak at around 10 keV, and a large amount of stripped electrons is generated. Since the stripped electron is largely deflected by the strong By near the EG and intercepted by the EG and the SG, the power loss on these grids is not affected by the non-uniform transverse magnetic field. On the other hand, the power loss on the GG

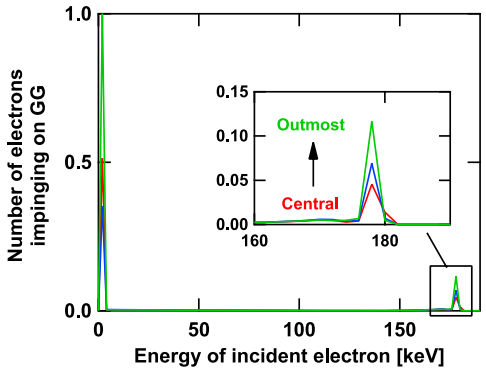

Fig. 5 Number of electrons impinging on GG as a function of electron energy in non-uniform magnetic field.

increases by closing to the grid edge in non-uniform magnetic field. Figure 5 shows the number of electrons incident on the GG as a function of the electron energy. There are two peaks at the low energy region (< 5 keV) and the high energy region (= 178 keV), which correspond to the stripped electron produced near the GG and the secondary electron ejected from the EG and the SG, respectively. Most of incident electrons is the low energy stripped electron, but the heat loading on the GG becomes higher than that on the EG and the SG due to high energy secondary electron. In Fig. 5, the number of secondary electrons increases near the outmost aperture, resulting in higher power loss. This indicates that the secondary electrons are more likely to be intercepted by the GG due to the stronger transverse magnetic field.

4.2 Influence of non-uniformity in plasma density on grid heat loading

It was assumed that the plasma density decreases at the periphery of the plasma chamber in order to estimate the beam optics of H^- extracted from non-uniform plasma. Figure 6 (a) shows an assumed profile of H^- current density. The H^- current density was assumed to be uniform in the central region including 8 apertures in the center and reduce by 30% at the outmost aperture. Figure 6 (b) shows the divergence of each beamlet in uniform and non-uniform plasma cases at the extraction voltage of 9.6 kV and the acceleration voltage of 178 kV. The H^- current density in the non-uniform plasma case was obtained by multiplying the factor with that in the uniform case, as the total current becomes the same for the uniform plasma. In Fig. 6 (b), the divergence becomes large and constant in the central region, but slightly decreases in the edge region where the current density also changes. This shows that perveance condition of beamlets strongly depends on the plasma density profile. The power loss on the EG is shown in Fig. 6 (c). The power loss on the EG has the same characteristic as the divergence. Namely, it becomes constant in the uniform current density region and decreases in the outer region. This indicates that some fraction of the H^-

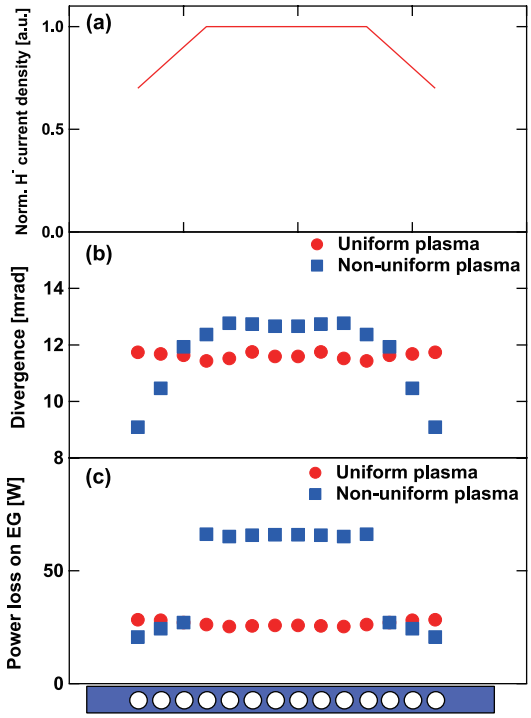

Fig. 6 (a) Normalized H^- current density, (b) divergence of each beamlet, and (c) power loss of particles on EG. H^- current density in non-uniform plasma case was estimated by multiplying factor with that extracted from uniform plasma profile.

extracted from non-uniform plasma is intercepted by the EG due to its high divergence and dissipates high power on the EG.

Acknowledgements

This research was supported by Japan Society for the Promotion of Science and NIFS (NIFS12ULRR015).

[1] Y. Takeiri, K. Ikeda, Y. Oka, K. Tsumori, M. Osakabe, K. Nagaoka, O. Kaneko, E. Asano, T. Kondo, M. Sato, M. Shibuya and S. Komada, Rev. Sci. Instrum. **77**, 03A523 (2006).
[2] A. Kojima, M. Hanada, A. Hilmi, T. Inoue, K. Watanabe, M. Taniguchi, M. Kashiwagi, N. Umeda, H. Tobari, S. Kobayashi, Y. Yamamo and L.R. Grisham, Rev. Sci. Instrum. **83**, 02B117 (2012).
[3] R. Hemsworth, H. Decamps, J. Graceffa, B. Schunke, M. Tanaka, M. Dremel, A. Tanga, H.P.L de Esch, F. Geli, J. Milnes, T. Inoue, D. Marcuzzi, P. Sonato and P. Zaccaria, Nucl. Fusion **49**, 045006 (2009).
[4] T. Morishita, K. Miyamoto, Y. Fujiwara, M. Handa, T. Kitagawa, M. Kashiwagi, Y. Okumura and K. Watanabe, Rev. Sci. Instrum. **73**, 1064 (2002).
[5] M. Kisaki, M. Hanada, M. Kamada, Y. Tanaka, K. Kobayashi and M. Sasao, AIP Conf. Proc. **1097**, 344 (2009).
[6] P. Agostinetti, V. Antoni, M. Cavenago, G. Chitarin, H. Nakano, N. Pilan, G. Serianni, P. Veltri, Y. Takeiri and K. Tsumori, AIP Conf. Proc. **1390**, 526 (2011).
[7] M. Hanada, Y. Fujiwara, K. Miyamoto, N. Miyamoto, Y. Okumura and K. Watanabe, Rev. Sci. Instrum. **69**, 947 (1998).
[8] M. Hamabe, Y. Takeiri, K. Ikeda, Y. Oka, M. Osakabe, K. Tsumori, E. Asano, T. kawamoto and O. Kaneko, Rev. Sci. Instrum. **72**, 3237 (2001).
[9] G. Fubiani, H.P.L. de Esch, A. Simonin and R.S. Hemsworth, Phys. Rev. ST Accel. Beams **11**, 014202 (2008).
[10] OPERA-3d, Vector Field Co. Ltd.
[11] J. Pamela, Rev. Sci. Instrum. **62**, 1163 (1991).